Crystal field and microwave absorption spectra in tetragonal $HoBa_2Cu_3O_x$ ($x=6.0$ and 6.3)

Z. A. Kazei,* V. V. Snegirev, and N. P. Danilova
Moscow State University, Moscow 119992, Russia

M. Goiran
Laboratoire Nationale des Champs Magnetiques Pulses, 31432 Toulouse, France

V. Nekvasil
Institute of Physics, CAS, Cukrovarnicka 10, CS-16253 Praha 6, Czech Republic

L. P. Kozeeva and M. Yu. Kameneva
Nikolaev Institute of Inorganic Chemistry, Siberian Branch, Russian Academy of Sciences, Novosibirsk 630090, Russia
(Received 27 July 2010; revised manuscript received 1 October 2010; published 27 October 2010)

The microwave resonance absorption at wavelengths 871, 406, 305, and 118 μm (frequencies 344, 739, 984, and 2540 GHz) in tetragonal layered perovskites $HoBa_2Cu_3O_x$ ($x\approx 6.0, 6.3$) in pulsed magnetic fields up to 40 T has been observed. This absorption is caused by the electronic transitions between low-lying levels of the Ho^{3+} ion in the crystal field. The positions and intensities of the tetragonal symmetry allowed absorption lines for the crystal with $x=6.0$ in the magnetic field oriented along the principal tetragonal axes are adequately described in terms of the available crystal field parameters. To explain the symmetry forbidden absorption lines, it is necessary to take into account the effect of the inhomogeneous orthorhombic and monoclinic components of the crystal field as well as an effective exchange field from the ordered Cu^{2+} subsystem at the Ho^{3+} sites. The origin of the local deviations from the ideal tetragonal symmetry are ascribed to disorder in the oxygen subsystem This disorder and consequently also its impact on the absorption spectra is more pronounced in the crystal with $x=6.3$.

DOI: 10.1103/PhysRevB.82.134444 PACS number(s): 71.70.−d, 75.30.−m, 75.40.Cx

I. INTRODUCTION

In $RBa_2Cu_3O_x$ compounds[1,2] (R—rare-earth ion or yttrium), the rare-earth and superconducting subsystems are known to weakly interact, which is evidenced by magnetic ordering in the rare-earth subsystem observed both in superconducting and in nonsuperconducting samples at low temperatures. The trivalent rare-earth ions are located at the structure sufficiently close to the CuO_2 "superconducting planes" and can serve as a local probe, sensitive to the symmetry of its environment and the charge-density distribution. The changes in the symmetry and charge distribution significantly influence the crystal field (CF) splitting of the $4f^n$ electronic structure of the rare-earth ion. The crystal field and magnetic excitations in layered perovskites were investigated in many neutron[3–6] and optical absorption[7–9] works. However, the reported electronic structures of rare-earth ions are not always entirely compatible with the results of detailed investigations of the magnetic properties of the crystals in applied magnetic fields (see, e.g., Ref. 10). One of the suggested causes for this discrepancy are the local deviations from the ideal tetragonal symmetry. The structure of layered perovskite crystals is imperfect, the disorder in the oxygen subsystem can give arise the inhomogeneous (i.e., some variation in the tetragonal CF parameters across the sample) and low-symmetric components of the CF, primarily of the second order ($B_2^2O_2^2$ type), the contribution to which from the neighboring charges decreases slowly with an increase in distance. The disorder-induced low-symmetry CF components are expected to strongly influence the magnetic behavior of non-Kramers paramagnets such as $HoBa_2Cu_3O_x$.

A singlet paramagnet $HoBa_2Cu_3O_x$, one of the most interesting objects of this type within the $R123$ family, exhibits a coupled electron-nuclear ordering at very low temperature.[11] Experimental study of the magnetic properties of $HoBa_2Cu_3O_x$ ($x\approx 6.3$) crystal in low and high magnetic fields revealed the intimate relation between the low-energy part of the electronic structure and the peculiarities of the magnetic behavior: the value and sign of the magnetic anisotropy, the change in the easy magnetization axis induced by varying temperature or magnetic field, a manifestation of the energy level crossing effect in high magnetic field, etc.[10]

In particular, the calculation of the Zeeman effect and magnetic properties of the $HoBa_2Cu_3O_x$ compounds considering the parameters of the CF determined from the neutron experiments predicts the crossover of the energy levels of the Ho^{3+} ions for the magnetic field $\mathbf{H}\|[001]$.[12,13] However, merely "hints" of the expected magnetic anomalies were observed in the experiment.[10] It implies that the observed magnetic behavior of the $HoBa_2Cu_3O_x$ crystal at low temperatures is not in full agreement with the electronic structure of the Ho^{3+} ion obtained in Refs. 3–5; i.e., the CF analysis should be refined.

Aiming at this refinement we investigated in this work the microwave (MW) absorption spectra in high magnetic fields, providing direct information on the electronic structure of the rare-earth ion, i.e., the energy spacing between the lowest-energy CF levels, value and anisotropy of the doublet g factors, and matrix elements of the relevant operators.[14] The experimental MW absorption data are then compared to the results of numerical calculations based on the CF formalism.

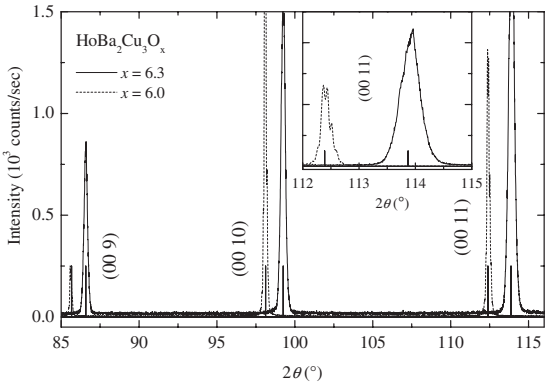

FIG. 1. X-ray patterns of the $HoBa_2Cu_3O_x$ crystal before ($x=6.9$, $c=11.741$ A) and after ($x=6.0$, $c=11.841$ A) annealing in vacuum at 670 °C. The calculated positions of the diffraction peaks are shown by vertical bars. The inset shows the diffraction peaks (00 11) in the larger scale.

In two following sections we describe the experimental technique and present experimental data in pulsed magnetic fields. The crystal field model used and the Ho^{3+} electronic structure in $HoBa_2Cu_3O_x$ is described in Sec. IV. The results of the CF analysis of the MW absorption spectra are discussed in Sec. V.

II. SAMPLES AND EXPERIMENTAL TECHNIQUES

The $HoBa_2Cu_3O_x$ single crystals were grown by the flux method from alumina crucibles. The "as-grown" crystals were then annealed in air or in vacuum at temperatures 900 °C and 650 °C, respectively, and were rapidly quenched down to room temperature in order to transform the samples to the tetragonal phase. The iodometric titration method showed that the oxygen content in the crystals after such a thermal treatment was $x=6.3$ and 6.0, respectively. According to chemical and electron-probe microanalyses, the cation ratio in these crystals was 1:2:3 within the limits of the experimental error. The Al weight concentration in the crystals did not exceed 0.5%, and their composition can be written as $HoBa_2Cu_{3-y}Al_yO_x$ ($y \leq 0.1$).

X-ray analysis of the crystals before and after annealing was carried out in order to determine admixture phases, a change in the lattice parameters and the width of diffraction peaks. The latter indicates the variation in the lattice parameters a and c (i.e., the oxygen index) across the sample. X-ray patterns of the Ho123 crystal before and after annealing (Fig. 1, the calculated line positions are shown by vertical bars) demonstrate the increase in the parameter c after annealing in accordance with the literary data.[15] As a result, the diffraction peak (00 11) for the annealed crystal is displaced by about $\Delta(2\theta)=1.5°$ (inset in Fig. 1). In addition, diffraction peaks become considerably (two to three times) narrower after annealing in vacuum as compared to the peaks for the as-grown crystal.

The crystals were found to absorb strongly at the wavelengths used in experiments. Therefore, we used thin plates, whose thickness was about 0.1 mm along the tetragonal axis; their sizes in the plane perpendicular to the tetragonal axis were 3×4 mm^2. Our experience demonstrates that it is impossible to measure MW absorption spectra in a high magnetic field along the hard magnetization axis on a free crystal because of a torque that appears at a small field deviation. To prevent samples from breaking during a field pulse we had to place them in an epoxy resin drop.

The pulsed measurements were performed using equipment at the Laboratoire Nationale des Champs Magnetiques Pulses (Toulouse, France). The field was generated at the discharge of a capacitor battery through a copper coil. The maximum field $H_{max}=36$ T was reached in 70 ms, and the total duration of the pulse was about 300 ms (for details see Ref. 16). The MW absorption spectra were investigated in the Faraday geometry at wavelengths 871, 406, 305, and 118 μm (frequencies 344, 739, 984, and 2540 GHz) in magnetic fields up to 36 T and temperatures ranging from 4.2 to 40 K. The excitations in the far infrared region were obtained using the Fabry-Perot cavity with optical pumping by a CO_2 laser. The deviation of the field from the tetragonal [001] axis under our experimental conditions was the same for all wavelengths and temperatures and was no more than $\sim 2° - 3°$.

III. MICROWAVE ABSORPTION SPECTRA

The intensity of 871, 406, 305, and 118 μm microwave radiation passed through the $HoBa_2Cu_3O_6$ crystal (transparency) for various temperatures is shown in the upper panels of Figs. 2–5 as a function of the magnetic field applied along the [001] tetragonal axis. For each wavelength, the spectra for various temperatures are given in the same scale and are shifted along the ordinate axis by a certain value. The absorption spectra at various wavelengths have some common features.

Let us consider specific features of the spectra at the wavelength of 871 μm ($f=344$ GHz, Fig. 2) in more detail. At $T=4.2$ K, two resonance lines $\underline{a}$ and $\underline{b}$ of different intensities are observed near $H=2$ and 19 T. These lines correspond to transitions from the ground level of the Ho^{3+} ion to the sublevels of the excited doublet at 14 K split in the magnetic field since their intensities decrease with increasing temperature. The low-field absorption line $\underline{a}$ has an asymmetric shape and a long tail from the side of low fields (see inset in Fig. 2). The weaker absorption line $\underline{c}$ near 4 T is associated with the transition from the lower sublevel of the doublet at 14 K; the relative intensity of this line increases with temperature. The absorption spectrum at a wavelength of 406 μm ($f=739$ GHz, Fig. 3) exhibits a qualitatively similar behavior: lines $\underline{d}$ and $\underline{e}$ are associated with the transitions from the ground level and high field line $\underline{e}$ becomes wider. The weaker lines $\underline{d}'$, $\underline{f}$, and $\underline{g}$ are attributed to the transitions from the low-lying exited levels.

Pronounced lines associated with the transitions from excited levels are observed in the spectra at wavelengths 305 and 118 μm ($f=984$ and 2540 GHz, Figs. 4 and 5). In the spectra at wavelength of 305 μm, two absorption lines $\underline{h}$, $\underline{h}'$ attributed to the transitions from the ground (or low-lying excited levels) merge into a wide line whereas the transitions from the excited levels result in the absorption lines $\underline{i}$ and $\underline{j}$.

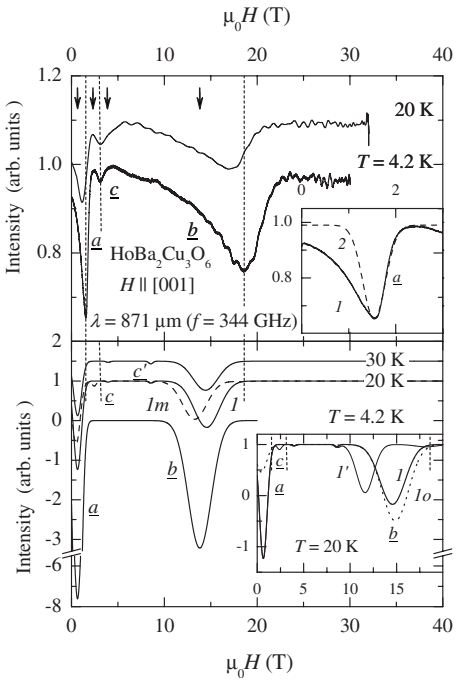

FIG. 2. Experimental (upper panel) and calculated (lower panel) MW absorption spectra of the $HoBa_2Cu_3O_{6.0}$ crystal in the pulsed magnetic field directed along the tetragonal axis at 871 μm (f =344 GHz, spectra for different temperatures are shifted along the ordinate by a certain value). Lines $\underline{a}$-$\underline{c}$ correspond to the transitions between the Ho^{3+} energy levels marked in lower panel of Fig. 7. The calculations have been performed for the set 2 of the CF parameters without (full curves) and with inclusion of a small monoclinic (B_2^1=120 K, dashed curve 1m) and orthorhombic (B_2^2 =40 K, dotted curve 1o) CF components as well as with a small deviation ($\Delta\theta$=10°, full thin curve 1′) out of the tetragonal axis. The calculated positions of the absorption lines are marked by an arrow in the experimental spectra. The inset shows the approximation of the experimental absorption line at 2 T (curve *1*) by Gaussian shape line (curve *2*).

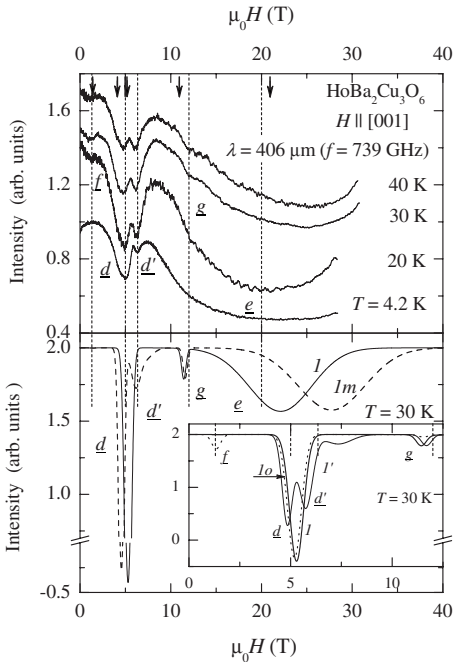

FIG. 3. Experimental (upper panel) and calculated (lower panel) MW absorption spectra of the $HoBa_2Cu_3O_{6.0}$ crystal in the pulsed magnetic field directed along the tetragonal axis at 406 μm (f =739 GHz, spectra for different temperatures are shifted along the ordinate by a certain value). Lines $\underline{d}$-$\underline{g}$ correspond to the transitions between the Ho^{3+} energy levels marked in upper panel of Fig. 7. The calculations have been performed for the set 2 of the CF parameters without (full curves) and with inclusion of a small monoclinic (B_2^1=120 K, dashed curve 1m) or orthorhombic (B_2^2=40 K, dotted curve 1o) CF components as well as with a small deviation ($\Delta\theta$=10°, full thin curve 1′) out of the tetragonal axis. The calculated positions of the absorption lines are marked by an arrow in the experimental spectra.

And in the spectra at wavelength of 118 μm, two absorption lines $\underline{k}$ and $\underline{l}$ exhibiting the opposite dependence of the intensity on the temperature can be connected to the transitions from the ground and exited levels, respectively.

The investigations of the crystal with x=6.3 at the same wavelengths reveal strong nonresonance absorption, which is likely due to an increase in charge carriers. Resonance absorption was reliably observed and investigated at the wavelength of 871 μm (see a typical spectrum in Fig. 6). Weak resonance lines $\underline{a}$ and $\underline{c}$, located symmetrically with respect to the minimum at 2 T, are seen against the large nonresonance absorption background exhibiting a wide maximum in the region 5–10 T. Although these lines are not clearly resolved in fields, they are well reproduced in consecutive magnetic field "shots." Also, there is a significant absorption in the field interval 0–1.5 T as compared to the crystal with x=6.0. The comparison of the spectra for the crystals with x=6.0 and 6.3 shows that the relative intensity of line $\underline{c}$ increases with the oxygen content and approaches the intensity of line $\underline{a}$.

IV. THEORETICAL BACKGROUND

To calculate the absorption spectra of the tetragonal crystals $HoBa_2Cu_3O_x$ in the high magnetic field, we used a Hamiltonian including the crystal field Hamiltonian, H_{CF}, and the Zeeman term, H_Z.

$$H = H_{CF} + H_Z. \tag{1}$$

The CF term is written within a system of x,y,z axes parallel to the [100], [010], and [001] axes of the lattice cell, respectively:

$$H_{CF} = \alpha_J B_2^0 O_2^0 + \beta_J (B_4^0 O_4^0 + B_4^4 O_4^4) + \gamma_J (B_6^0 O_6^0 + B_6^4 O_6^4), \tag{2}$$

where O_n^m, B_n^m, and $(\alpha_J, \beta_J, \gamma_J)$ are the Stevens operators, CF parameters, and Stevens parameters, respectively. The interaction with the applied magnetic field **H** is described by the Zeeman term,

$$H_Z = -g_J \mu_B \mathbf{H} \cdot \mathbf{J}, \tag{3}$$

where **J** is the angular momentum operator for the Ho^{3+} ion, and g_J and μ_B are the Landé factor and the Bohr magneton, respectively. Neutron investigations of magnetic excitations

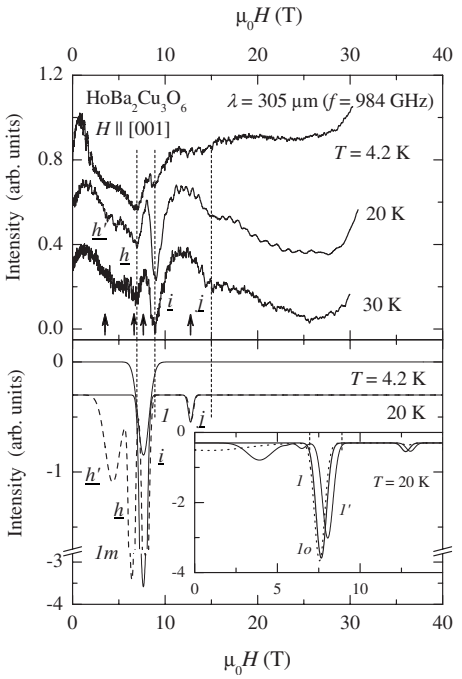

FIG. 4. Experimental (upper panel) and calculated (lower panel) MW absorption spectra of the $HoBa_2Cu_3O_{6.0}$ crystal in the pulsed magnetic field directed along the tetragonal axis at 305 μm (f =984 GHz, spectra for different temperatures are shifted along the ordinate by a certain value). Lines $\underline{h}$-$\underline{j}$ correspond to the transitions between the Ho^{3+} energy levels marked in lower inset of Fig. 7. The calculations have been performed for the set 2 of the CF parameters without (full curves) and with inclusion of a small monoclinic (B_2^1 =120 K, dashed curve 1m) and orthorhombic (B_2^2=40 K, dotted curve 1o) CF components as well as with a small deviation ($\Delta\theta$ =10°, full thin curve 1′) out of the tetragonal axis. The calculated positions of the absorption lines are marked by an arrow in the experimental spectra.

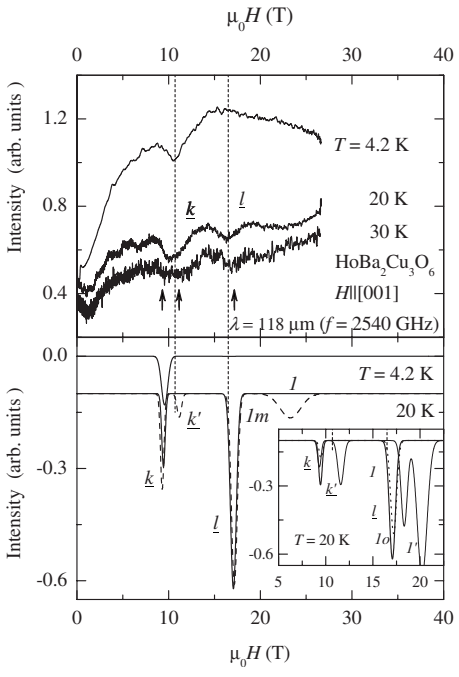

FIG. 5. Experimental (upper panel) and calculated (lower panel) MW absorption spectra of the $HoBa_2Cu_3O_{6.0}$ crystal in the pulsed magnetic field directed along the tetragonal axis at 118 μm (f =2540 GHz, spectra for different temperatures are shifted along the ordinate by a certain value). Lines $\underline{k}$-$\underline{l}$ correspond to the transitions between the Ho^{3+} energy levels marked in upper inset of Fig. 7. The calculations have been performed for the set 2 of the CF parameters without (full curves) and with inclusion of a small monoclinic (B_2^1 =120 K, dashed curve 1m) and orthorhombic (B_2^2=40 K, dotted curve 1o) CF components as well as with a small deviation ($\Delta\theta$ =10°, full thin curve 1′) out of the tetragonal axis. The calculated positions of the absorption lines are marked by an arrow in the experimental spectra.

and interactions in the $HoBa_2Cu_3O_x$ compounds show that the exchange interactions involving the Ho ions are weak[11,17] and do not lead, according to our analysis, to a noticeable effect in the MW absorption spectra. Note that the effective fields from two Cu sublattices cancel each other at the Ho^{3+} sites for a simple collinear magnetic structure according to the symmetry arguments.[18–20] For a magnetic structure with canted Cu^{2+} magnetic moments, an effective field at the Ho^{3+} sites from the ordered Cu^{2+} subsystem, H_{Cu}, perpendicular to the tetragonal axis can appear.

Various sets of the tetragonal CF parameters and their applicability to the description of the existing experimental $HoBa_2Cu_3O_x$ data were discussed in Ref. 10. The data for crystals with $6.0<x<6.3$ indicate the presence of the orthorhombic or even lower symmetry CF components.[10] In the case of the orthorhombic CF, Hamiltonian (2) is supplemented by four additional terms $B_n^2O_n^2$ (n=2,4,6) and $B_6^6O_6^6$; the largest effect is here attributed to the second-order term $B_2^2O_2^2$. Similarly, the monoclinic CF components are represented by the second-order term $B_2^1O_2^1$ in the following.

The energy levels E_i and wave functions $|i\rangle$ of the Ho^{3+} ion are obtained by numerically diagonalizing the total perturbation Hamiltonian, Eq. (1). The relative intensity int(i,j) of the resonance absorption line, corresponding to transition between the CF levels i and j of the ground multiplet, is calculated using the formula,

$$\mathrm{int}(i,j) \sim g_J^2\mu_B^2 \sum_i \sum_{j>i} (f_i - f_j)\langle i|J_\alpha|j\rangle\langle j|J_\alpha|i\rangle g(E) \quad (\alpha = x,y). \tag{4}$$

Here, the difference between the Boltzmann factors f_m =$\exp(-E_m/k_BT)/Z$; $[m=i,j;\ Z=\Sigma_i\exp(-E_i/k_BT)]$ accounts for the different populations of the levels i and j. In the longitudinal geometry $\mathbf{k}\|\mathbf{H}$ and for the magnetic field orientated along the tetragonal [001] axis, the formula contains the matrix elements $\langle i|J_\alpha|j\rangle(\alpha=x,y)$. In our experiment the line shape $g(E)$ is approximated by the Gaussian function $g(E)=\exp[-(E-E_{ij})^2/2\sigma_E^2]/(\sqrt{2\pi}\sigma_E)$, except for a low-field tail (see dashed curve in inset of Fig. 2). The magnetic field linewidth $\sigma=\sigma_H=\sigma_E/(\partial E_{ij}/\partial H)$ is determined by the energy linewidth σ_E and a derivative $\partial E_{ij}/\partial H$, i.e., by the dependence of the energy difference $E_{ij}=(E_j-E_i)$ on the magnetic field near the resonance field H_{ij}. The energy linewidth σ_E was determined from the $\underline{a}$ resonance line in the 871 μm experimental spectrum. We did not take into account the

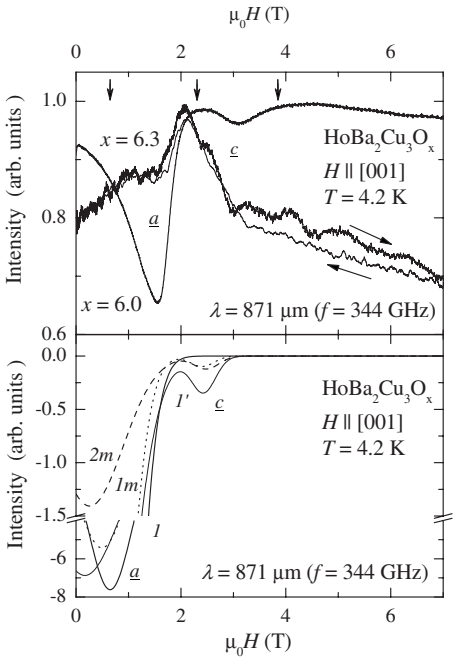

FIG. 6. Experimental (upper panel) and calculated (lower panel) MW absorption spectra of the $HoBa_2Cu_3O_x$ (x=6.0,6.3) crystals in the pulsed magnetic field directed along the tetragonal axis at 871 μm (f=344 GHz) and 4.2 K. Lines a-c correspond to the transitions between the Ho^{3+} energy levels marked in lower panel of Fig. 7. The calculations have been performed for the set 2 of the CF parameters without (solid curve *1*) and with inclusion of the monoclinic (dashed curve $1m$-B_2^1=120 K, dotted curve $2m$-B_2^1=170 K) CF component and molecular field from the Cu^{2+} subsystem (H_{Cu} =1.5 T, full thin curve $1'$). The calculated positions of the absorption lines are marked by an arrow in the experimental spectra.

variation in the shape and width of the lines with temperature. Owing to the finite linewidth σ_H, a noticeable absorption can be observed in the region $[H_{ij}-\sigma_H, H_{ij}+\sigma_H]$; therefore, wide asymmetric lines have been observed when the derivative $\partial E_{ij}/\partial H$ is small.

To calculate the resonance absorption spectra we used two different approaches. First, we found the resonance fields H_{ij} at which the condition $E_j-E_i=\hbar c/\lambda$ was satisfied, then calculated the integrated intensities of the absorption lines at H_{ij} by Eq. (4) at $g(E)=1$, and, finally, "smeared" the absorption intensity according to the experimental $g(E)$ line shape. Within the second method, the matrix elements $\langle i|J_\alpha|j\rangle$ appearing in Eq. (4) were calculated at various values of H with a small step ΔH=0.01 T for each pair of levels i and j, then multiplied by the Boltzmann factor and the $g(E)$ function; the latter takes into account the proximity of the energy difference E_j-E_i to the resonance condition. In most cases (in the absence of the "quasiresonance" absorption), the results obtained by the two methods practically coincide. The second method, which is more sensitive to the $g(E)$ line shape, was used to calculate the absorption line intensities for transitions between the crystal field split levels whose energies are very close to (but do not exactly meeting) the resonance condition $E_i-E_j=\hbar c/\lambda$ (quasiresonance absorption) and whose matrix elements are large.

Taking into account the pulse duration in our experiments we consider the magnetization regime as being close to adiabatic for the upsweep and intermediate for the downsweep. Analyzing the experimental data we thus have to take into account the magnetocaloric effect (MCE). However, the temperature change is small enough for singlet paramagnets at intermediate filed and low temperatures, where the susceptibility $\chi(T)_{H=0}$ changes weakly. We estimated the MCE in the magnetic field $\mathbf{H}\|[001]$ using the experimental magnetic data for the $HoBa_2Cu_3O_{6.3}$ crystal.[10] At start temperatures 4.2 and 20 K, the crystal heating is within (2–3) K in fields below 10 T and does not exceed 8 K at the maximum field.

V. DISCUSSION OF RESULTS

A. Crystal field parameters and the electronic structure of the Ho^{3+} ion

To calculate the Zeeman effect and the resonance absorption spectra we first analyzed the available information on the CF for the $HoBa_2Cu_3O_x$ compounds. The CF parameters for the family of layered perovskites $RBa_2Cu_3O_x$ were first predicted using the superposition model for compounds with various R ions and different oxygen content,[21] and subsequently refined in numerous experimental studies. In most cases, an experimental information on the CF splitting of the ground multiplet was provided by the inelastic neutron-scattering (INS) measurement,[3–6] the splitting of the excited multiplets by the infrared absorption studies.[7–9]

The $HoBa_2Cu_3O_x$ compounds with various oxygen contents were studied in detail using the INS.[3–5] The J mixing as well as the intermediate coupling, neglected in earlier CF studies,[3,4] was taken into account in Ref. 5. Within the operator equivalent formalism described in Sec. IV, neglecting the J mixing as well as the intermediate coupling, this set of CF parameters (set 3) had to be modified to account properly for the experimental CF splitting.[10] The resulting CF parameters (set 2 in Table I) are used in the following. We note that the set 1 is very close to the CF parameters available for $DyBa_2Cu_3O_{6.0}$.[22] It is interesting that parameter B_2^0 has different values in sets 1 and 3; its value in set 3 is in better agreement with the experimental value of the magnetic anisotropy at high temperatures.

The INS data on the tetragonal $HoBa_2Cu_3O_{6.0}$ show that the Ho^{3+} ground state is a singlet and the first excited state is a doublet at about 14 K.[3–5] The evolution of the INS spectra with the oxygen content x demonstrates that the doublet splits into singlets in the orthorhombic compounds ($x>6.4$) and the splitting increases with increasing x. The principle features of the INS spectra can be rather well described in terms of the magnetic dipole matrix elements within the tetragonal symmetry CF eigenstates. At the same time our magnetic data indicate that the available CF analyses require further refinement.[10] This is particularly true for the wave functions calculated using the best-fit CF parameters derived from the available INS spectra.[3–5] Though these wave functions describe the transition intensities adequately, this solution seems not to be unique.

The calculated splitting of the energy levels of the Ho^{3+} ion (five lower levels) in $HoBa_2Cu_3O_6$ for the CF parameters from Ref. 10 (the set 2 in Table I) in the magnetic field oriented along the [001] axis is shown in Fig. 7. At H=0, the

TABLE I. Various sets of the CF parameters for $R\mathrm{Ba_2Cu_3O_x}$ in the operator equivalent formalism.

Compound		B_2^0 (K)	B_2^2 (K)	B_4^0 (K)	B_4^2 (K)	B_4^4 (K)	B_6^0 (K)	B_6^2 (K)	B_6^4 (K)	B_6^6 (K)	Ref.
$\mathrm{DyBa_2Cu_3O_6}$		183		−275		1313	21.6		583		22
$\mathrm{HoBa_2Cu_3O_6}$	Set *1*	240.5		−331.2		1499	39.6		1296		3
$\mathrm{HoBa_2Cu_3O_7}$	Set 1*o*	241	104	−317	22	1465	40	−25	1211	−17	4
$\mathrm{HoBa_2Cu_3O_6}$	Set *2*	40.3		−298		1643	39.6		1296		10
$\mathrm{HoBa_2Cu_3O_6}$	Set *3*	40.7		−49.1		2043	2.7		952		5

total splitting of the ground J multiplet of the Ho^{3+} ion is about 900 K (74 meV) in both the tetragonal and orthorhombic structures. For these CF parameters, the lowest singlet and doublet levels are separated by a gap of about 14 K, in accordance with the experiment, and their wave functions in the (J,J_z) representation have the form $\{-0.52|6\rangle-0.48|2\rangle+0.48|-2\rangle+0.52|-6\rangle\}$ and $\{0.62|\pm7\rangle+0.75|\pm3\rangle+\cdots\}$ (Table II).

The ground-singlet energy decreases weakly in the magnetic field $\mathbf{H}\|[001]$ while the first excited doublet is strongly split. As a result, the lower component of the split doublet,

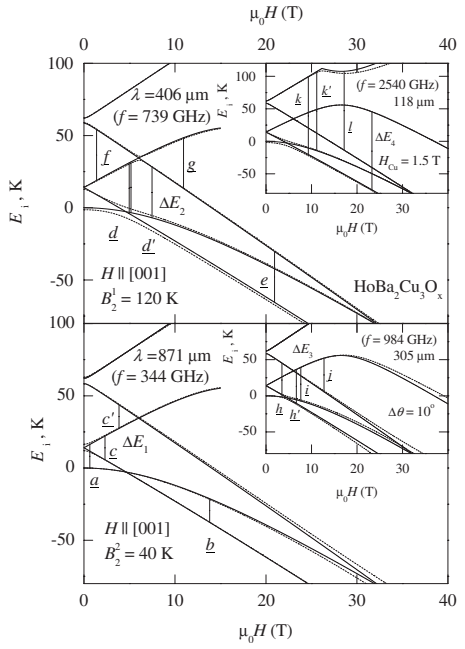

FIG. 7. Zeeman effect in the $\mathrm{HoBa_2Cu_3O_6}$ crystal for the magnetic field directed along the tetragonal axis as calculated disregarding the pair interactions. The dotted lines show the effect of the monoclinic (upper panel, B_2^1=120 K) and orthorhombic (lower panel, B_2^2=40 K) CF components as well as the molecular field from the Cu^{2+} subsystem (upper inset, H_{Cu}=1.5 T) and small magnetic field deviation out of the tetragonal axis (lower inset, $\Delta\theta$ =10°). The allowed transitions between the energy levels of the Ho^{3+} ion at wavelengths 871 and 305 μm (f=344 and 984 GHz; lower panel ΔE_1=16.4 K, lower inset ΔE_3=46.8 K) and wavelengths 406 and 118 μm (f=739 and 2540 GHz; upper panel ΔE_2=35.2 K K, upper inset ΔE_4=121.0 K) correspond to the absorption lines shown in Figs. 2–5.

which has a large $|M_z\rangle$ magnetic-moment component, approaches and crosses the ground singlet in the critical field H_c=4 T. In terms of the Hamiltonian used, a gap between the crossed levels is absent at the crossover for a magnetic field oriented strictly along the [001] axis, and the gap is small (less than 3 K) for a field deviation not exceeding 10° (low inset in Fig. 7).

The level crossing without a gap should be accompanied by pronounced anomalies in the $M(H)$ and $dM/dH(H)$ curves at low temperatures. Pronounced magnetic anomalies in high magnetic field due to the crossover have been observed experimentally in a number of tetragonal R zircons including the holmium vanadate $HoVO_4$.[23] The magnetic anomalies in $\mathrm{HoBa_2Cu_3O_x}$ near level crossing were expected to be somewhat less pronounced in a comparison to the vanadate since the energy of the singlet state is in our case characterized by a stronger field dependence dE_1/dH_z=0.87 near H_c. The noticeable contribution of the $|\pm6\rangle$ states to the wave function of the ground singlet leads to a faster increase in the magnetization for the case of $\mathbf{H}\|[001]$ in fields below H_c. However, the expected pronounced magnetic anomalies were absent in the $\mathrm{HoBa_2Cu_3O_x}$ ($x\approx6.3$) data.[10]

A finite gap near the critical field H_c is known to smooth noticeably the magnetic anomalies in real crystals. The presence of the gap can be ascribed to additional interactions, not included in Hamiltonian, Eq. (1), properly mixing the tetragonal symmetry wave functions of the interacting levels. Taking into account the symmetry of the lowest energy eigenstates we discuss in the following interactions, which could possibly lead to such a mixing. The corresponding Hamiltonian should contain the operators J_x or J_y (or odd powers of these operators), mixing strongly the components $|\pm6\rangle$ and $|\pm7\rangle$ as well as the components $|\pm2\rangle$ and $|\pm3\rangle$ of the lowest energy eigenstates.

We consider two interactions possessing the required symmetry properties. First is a strong local symmetry lowering at the Ho^{3+} site due to a disorder in the oxygen subsystem. It is to be noted that the orthorhombic CF terms, described by even powers of J_x and J_y, do not mix the wave functions of the singlet and doublet and thus change only weakly the magnetic properties of $\mathrm{HoBa_2Cu_3O_x}$ along the hard axis.

The monoclinic component $B_2^1O_2^1$ strongly mixes the wave functions and decreases the magnitude of the anomaly in the $\chi_c(T)$ and $dM/dH(H)$ curves, bringing results of calculations closer to the experiment.[10] This term, written as $(J_zJ_x+J_xJ_z)/2$ in the operator equivalent notation, can appear if oxygen atoms in oxygen deficient planes are not completely

TABLE II. Energies E_i and wave functions $|i\rangle$ of the lower levels of the Ho^{3+} ion in the layered perovskite structure calculated for the set 2 of the tetragonal CF parameters and with inclusion of various low-symmetry CF components.

E_i (K)	$\|i\rangle = \sum_{M=8}^{-8} C_M\|M\rangle$
	Tetragonal CF, set 2
0	$\{-0.52\|6\rangle-0.48\|2\rangle+0.48\|-2\rangle+0.52\|-6\rangle\}$
14.0	$\{0.62\|7\rangle+0.75\|3\rangle-0.16\|-1\rangle-0.16\|-5\rangle\}$
14.0	$\{-0.16\|5\rangle-0.16\|1\rangle+0.75\|-3\rangle+0.62\|-7\rangle\}$
58.4	$\{0.36\|8\rangle+0.60\|4\rangle+0.08\|0\rangle+0.60\|-4\rangle+0.36\|-8\rangle\}$
62.1	$\{0.37\|8\rangle+0.60\|4\rangle-0.60\|-4\rangle-0.37\|-8\rangle+\cdots\}$
	Set 2, $B_2^2=40$ K
0	$\{(-0.51\|6\rangle-0.48\|2\rangle+0.48\|-2\rangle+0.51\|-6\rangle)+(-0.02\|8\rangle-0.03\|4\rangle+0.03\|-4\rangle+0.02\|-8\rangle+\cdots)\}$
12.6	$\{(-0.44\|7\rangle-0.53\|3\rangle+0.12\|-1\rangle+0.12\|-5\rangle)+(0.13\|5\rangle+0.13\|1\rangle-0.53\|-3\rangle-0.44\|-7\rangle)\}$
15.7	$\{(0.44\|7\rangle+0.53\|3\rangle-0.11\|-1\rangle-0.10\|-5\rangle)+(-0.10\|5\rangle-0.11\|1\rangle+0.53\|-3\rangle+0.44\|-7\rangle)\}$
	Set 2, $B_2^1=120$ K
−0.7	$\{(-0.51\|6\rangle-0.47\|2\rangle+0.47\|-2\rangle+0.51\|-6\rangle)+(-0.09\|7\rangle-0.10\|3\rangle+0.02\|-1\rangle+\cdots)+(0.02\|1\rangle-0.10\|-3\rangle-0.09\|-7\rangle+\cdots)+\cdots\}$
13.4	$\{(0.44\|7\rangle+0.53\|3\rangle-0.12\|-1\rangle-0.11\|-5\rangle)+(0.11\|5\rangle+0.12\|1\rangle-0.53\|-3\rangle-0.44\|-7\rangle)+(0.03\|6\rangle+0.02\|2\rangle+0.02\|-2\rangle+0.03\|-6\rangle)+\cdots\}$
14.4	$\{(0.43\|7\rangle+0.52\|3\rangle-0.11\|-1\rangle-0.11\|-5\rangle)+(-0.11\|5\rangle-0.11\|1\rangle+0.52\|-3\rangle+0.43\|-7\rangle)+(0.03\|6\rangle+0.02\|2\rangle+0.02\|-2\rangle+0.03\|-6\rangle)+\cdots\}$
	Set 2, $H_{Cu}=1.5$ T
−1.9	$\{(-0.49\|6\rangle-0.46\|2\rangle+0.46\|-2\rangle+0.49\|-6\rangle)+(-0.14\|7\rangle-0.17\|3\rangle+0.04\|-1\rangle+0.05\|-5\rangle)+(-0.05\|5\rangle-0.04\|1\rangle+0.17\|-3\rangle+0.14\|-7\rangle)+\cdots\}$
13.7	$\{(0.44\|7\rangle+0.53\|3\rangle-0.12\|-1\rangle-0.11\|-5\rangle)+(-0.11\|5\rangle-0.12\|1\rangle+0.53\|-3\rangle+0.44\|-7\rangle)+(0.02\|6\rangle+0.01\|2\rangle+0.01\|-2\rangle+0.02\|-6\rangle)+\cdots\}$
15.4	$\{(-0.41\|7\rangle-0.50\|3\rangle+0.11\|-1\rangle-0.10\|-5\rangle)+(-0.10\|5\rangle-0.11\|1\rangle+0.50\|-3\rangle+0.41\|-7\rangle)+(0.17\|6\rangle+0.15\|2\rangle-0.15\|-2\rangle-0.17\|-6\rangle)+\cdots\}$

ordered. In contrast to the higher order CF parameters the second order parameters B_2^0, B_2^2, and B_2^1 contain a significant contribution from distant ions, far from the coordination polyhedron. The distribution of this very low-symmetry field is accidental across the crystal so the parameter B_2^1 can vary in sign and value from one site to another; however an averaging over the crystal can result in a nonzero effect (see below). It is important to note that the CF parameter $B_2^1=120$ K, well describing the magnetic properties[10] and comparable in value with the B_2^0 parameter, shifts or splits very weakly, within 2–4 K, the energy spacings (except for the doublet at 720 K) but mixes strongly the wave functions of the lowest levels and thus changes significantly the magnetic properties of the examined Ho cuprate at low temperatures.

The second interaction, which could account for the absence of the pronounced magnetic anomaly, is the molecular field at the Ho^{3+} site arising from the magnetically ordered Cu^{2+} subsystem. Our analysis shows that the molecular field $H_{Cu}\approx 1.5$ T in the basal plane would bring the curves $\chi_c(T)$ and $dM/dH(H)$ along the hard axis [001] significantly closer to the experimental ones. Such molecular field is incompatible with the simple two sublattice antiferromagnetic structure without defects.[18–20] According to symmetry arguments the contributions to the effective fields at the rare-earth site from two Cu^{2+} sublattices cancel each other in the case of the collinear magnetic structure. The effective field can appear either for a magnetic structure with canted Cu^{2+} magnetic moments or, as in the case of R_2CuO_4, at a magnetic phase transition accompanied by a change in the magnetic structure.[24] It is known that the long antiferromagnetic order in the Cu^{2+} subsystem destroys quickly and transform into the spin-glasslike state when oxygen content increases above 6.4.[18] The model when the local molecular field H_{Cu} is oriented accidentally in the $(x\text{-}y)$ plane results in a nonzero contribution to magnetic properties along the tetragonal axis. Its contribution to the magnetic properties in the basal plane cancels out.

B. Microwave absorption spectra

The Zeeman effect calculations for the magnetic field $\mathbf{H}\|[001]$ using Eq. (1) were used to analyze the experimental MW absorption spectra of the $HoBa_2Cu_3O_6$ crystal at studied wavelengths. The energy-allowed transitions between the low-lying levels at the wavelengths 871 μm and 305 μm ($\Delta E_1=16.4$ K, $\Delta E_3=46.8$ K) and the wavelengths 406 μm and 118 μm ($\Delta E_2=35.2$ K, $\Delta E_4=121.0$ K) are shown by the vertical bars of corresponding lengths in the lower and upper panels of the Fig. 7, respectively. Only transitions whose relative intensity is at least 3% of the intensity of the main line are indicated. Note that the transitions in the tetragonal CF for a number of the experimental lines ($\underline{c}, \underline{d}', \underline{f}, \underline{h}, \underline{h}', \underline{k}'$) are symmetry forbidden—the wave functions of the relevant states i,j have no components that are mixed by the operator J_x (see Table II). However, these lines have the noticeable intensity when the CF Hamiltonian includes the monoclinic and/or orthorhombic components as well as the molecular field $H_{Cu}=1.5$ T from the ordered Cu^{2+} subsystem.

The orthorhombic component is responsible for the noticeable splitting of the first excited doublet (the dotted lines in the lower panel of Fig. 7, $B_2^2=40$ K), whereas the monoclinic component and molecular field lead to the appearance of a noticeable gap between the crossing levels near the crossover field H_c (the dotted lines in the upper panel and inset of Fig. 7, $B_2^1=120$ K, $H_{Cu}=1.5$ T). The number of the energy-allowed transitions between the low-lying levels of the Ho^{3+} ion is smaller for the field orientation $\mathbf{H}\|[100]$ (not shown in Fig. 7).

At the wavelength of 871 μm, two absorption lines are expected; they correspond to transitions between the crossing

levels and are located on either side of a crossover field $H_c = 4.2$ T. Higher photon energy allows to probe transitions to higher exited levels. At wavelengths 406, 305, and 118 μm, transitions from two quasidegenerate levels near H_c to the second, third, or fourth exited levels results in double lines ($\underline{d}$,$\underline{d}'$), ($\underline{h}$,$\underline{h}'$), and ($\underline{k}$,$\underline{k}'$), respectively (Figs. 3–5). We note that transitions from excited levels at more than 30–50 K, weakly populated at temperatures below 30 K, give rise to weak absorption lines in the MW absorption spectra (lines $\underline{f}$,$\underline{g}$,$\underline{j}$,$\underline{l}$).

The calculated absorption spectra of the $HoBa_2Cu_3O_6$ crystal for the field $\mathbf{H}\|[001]$ at the studied wavelengths (see lower panels of Figs. 2–5; positions of the experimental resonance lines $\underline{a}$-$\underline{l}$ are shown by the dashed vertical lines) allow us to explain the main features of the experimental spectra. The relative intensity, position, and width of the principle absorption lines are satisfactorily described in terms of the tetragonal CF (solid lines in Figs. 2–5). The field positions of the experimental lines are systematically higher at low temperatures (compare absorption lines $\underline{a}$ and $\underline{b}$ in the experimental and calculated spectra at 4.2 K in Fig. 2). At higher temperatures, the experimental absorption lines $\underline{a}$ and $\underline{b}$ move slightly to lower field and the difference decreases. This effect can be at least partly attributed to the magnetic relaxation in the pulsed field.

At the same time there is a number of lines in the experimental spectra (lines $\underline{c}$,$\underline{d}'$,$\underline{f}$,$\underline{h}$,$\underline{h}'$,$\underline{k}'$), which are forbidden in the tetragonal symmetry picture. The appearance of these lines can be attributed either to the effect of the lower symmetry CF components or to an uncompensated exchange field from the ordered Cu^{2+} subsystem, in both cases caused by disorder in the oxygen subsystem. This assumption is confirmed by the fact that forbidden line $\underline{c}$ is more intense in the crystal with $x=6.3$ (Fig. 6), for which disorder in the oxygen subsystem is known to be more pronounced.[25]

We analyzed in detail the effect of the low-symmetry CF components on the resonance absorption in the $HoBa_2Cu_3O_6$ crystal, namely, the B_2^1 monoclinic and B_2^2 orthorhombic components. Certain absorption lines (lines $\underline{c}$,$\underline{d}'$,$\underline{h}$,$\underline{h}'$,$\underline{k}'$) appear in the MW spectra only due to the finite B_2^1 monoclinic CF component. For most cases, the molecular field H_{Cu} causes the same effect. This is dictated by the character of the wave functions for the energy levels i and j involved in the transition (see Table II). We note that the magnetic field deviation $\Delta\theta = 10°$ from the tetragonal axis results in the similar effect as the presence of the monoclinic CF components (thin lines in Figs. 2–5). The orthorhombic CF components also cause the appearance of additional absorption lines (i.e., lines $\underline{f}$) and can change strongly the intensity of main absorption lines. The value and sign of the change depends on the value and the orientation of the local orthorhombic deformation axis along the $\langle 100\rangle$ or $\langle 110\rangle$ tetragonal axis as well as on the sign of the B_2^2 component.

The numerical simulation of the absorption spectra really indicates that the absorption line $\underline{c}$ of noticeable intensity appears at $B_2^1 \geq 120$ K. Its intensity slightly increasing with the increasing parameter B_2^1 in the range 120–170 K (compare curves $1m$ and $2m$ at $B_2^1 = 120$ K and 170 K, respectively, in the low panel of Fig. 6) while the intensity of the absorption line $\underline{a}$ decreases by a factor of 5 in this range. The inclusion of the molecular field H_{Cu} influences similarly, resulting in the noticeable absorption line $\underline{c}$ (curve $1'$, $H_{Cu} = 1.5$ T in Fig. 6). The numerical simulation reveals also the appearance of forbidden lines $\underline{d}'$ and $\underline{f}$ of a noticeable intensity at the wavelength of 406 μm due to the monoclinic and orthorhombic CF components, respectively (respective lines $1m$ and $1o$ in Fig. 3). The double line $\underline{h}$, $\underline{h}'$ in the absorption spectra at wavelength 305 μm (Fig. 4) is due to the monoclinic CF component. Similar calculations for the absorption spectra at wavelength 118 μm (Fig. 5), considering the low symmetry CF components, account for the appearance of the line $\underline{k}'$, a satellite to the line $\underline{k}$.

Analyzing the tetragonal symmetry forbidden lines in the experimental absorption spectra we focus on the contribution of the second-order orthorhombic and monoclinic CF terms $B_2^2O_2^2$ and $B_2^1O_2^1$, respectively. We discuss qualitatively the average effect of these components in the absorption spectra at 871 μm for the $HoBa_2Cu_3O_{6.3}$ crystal as compared to the $HoBa_2Cu_3O_6$ crystal. We note that, there are four different orthorhombic deformations of a tetragonal crystal for a given value $|B_2^2|$, equivalent to the elongation/compression along the [100], [010] or the [110], [1$\bar{1}$0] axes. The deformations along the [100] and [010] axes differ by the sign of the B_2^2 component; the deformations along the [110] and [1$\bar{1}$0] are equivalent to the former in the system rotated on 45° around of the z axis. Similarly, the monoclinic deformation for a given value $|B_2^1|$ may be oriented in the xz or $x'z$ planes.

The orthorhombic deformation along the [100] and [010] axes (upper panel of Fig. 8, curves $1o+$ and $1o-$) or the [110] and [1$\bar{1}$0] axes (not shown in Fig. 8) decreases noticeably the absorption intensity and moves the line $\underline{a}$ to the lower field $H \sim 0.4$ T. The effect of the B_2^2 is nonlinear and increases sharply for $B_2^2 \geq 50$ K. Averaging in sign and orientation of the B_2^2 component leads to the peak $1o$ which is wider and less intense compared to the peak 1 calculated neglecting the low-symmetry components. We note that difference $E_2 - E_1 = \hbar c/\lambda$ for line $\underline{a}$ does not exactly satisfy the resonance condition at large values of the B_2^2 and B_2^1 parameters but is rather close to it. Therefore, absorption remains significant because of the finite linewidth. In this case, the absorption spectra should be calculated without searching for a resonance field (the above-mentioned second method).

Similarly, the monoclinic deformation $B_2^1 = 120$ K in the xz or $x'z$ planes decreases the absorption intensity and moves the line $\underline{a}$ to the lower field resulting in the average curve $1m$ (lower panel of Fig. 8). Moreover, this deformation gives arise a weak line $\underline{c}$ near $H \sim 3.0$ T; its dependence on the B_2^1 value is discussed above (lower panel of Fig. 6). The effects of the monoclinic ($B_2^1 = 120$ K) and orthorhombic ($B_2^2 = \pm 40$ K) components are not additive (lower panel of Fig. 8).

The absorption line $\underline{b}$ reveals also the noticeable widening when the low-symmetry B_2^2, B_2^1 components are included. In accordance with the Zeeman effect (Fig. 7), the component $B_2^2 = \pm 50$ K influences weakly the position of the absorption line $\underline{b}$ near $H = 14$ T (inset to Fig. 8, curve $1o$) while the component $B_2^1 = 160$ K moves this line to the lower field (curve $1m$). Thus, the origin of the broad and weak absorp-

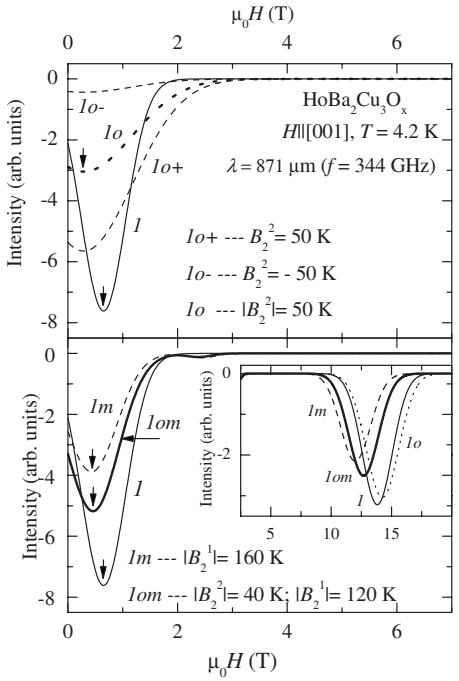

FIG. 8. MW absorption spectra of a $HoBa_2Cu_3O_x$ crystal in a pulsed magnetic field directed along the tetragonal axis at $T=4.2$ K and a wavelength of 871 μm ($f=344$ GHz) that were calculated for set 2 of CF parameters without (solid line *1*) and with inclusion of the orthorhombic deformation along the [100] and [010] axes (upper panel, $B_2^2=50$ K—curve 1*o*+, $B_2^2=-50$ K—curve 1*o*-, and $|B_2^2|=50$ K—curve 1*o*), monoclinic deformation in the *xz* and *x*′*z* planes (lower panel, $B_2^1=160$ K, curve 1*m*) and the combined effect of the monoclinic and orthorhombic deformation ($B_2^1=120$ K, $B_2^2=\pm 40$ K, curve 1*om*).

tion lines *a*,*b*,*c* in the experimental spectra of the $HoBa_2Cu_3O_{6.3}$ crystal in the field $H\|[001]$ in the range 0–2 T (Fig. 6) can be qualitatively explained considering an impact of the oxygen disorder, giving arise the orthorhombic and monoclinical symmetry terms in the CF Hamiltonian as well as the finite molecular field at the Ho^{3+} sites.

VI. CONCLUSIONS

We have shown that the magnetic behavior of $HoBa_2Cu_3O_x$ crystals ($x\approx 6.0, 6.3$) at low temperatures is not entirely consistent with predictions of a model based on the tetragonal symmetry CF at the Ho^{3+} sites. A number of resonance absorption lines at the wavelengths 871, 406, 305, and 118 μm ($f=344$, 739, 984, and 2540 GHz), resulting from the transitions between low-lying energy levels of the Ho^{3+} ion, are observed in the layered perovskite $HoBa_2Cu_3O_6$ in the presence of the magnetic field oriented along the tetragonal axis. The positions and intensities of the tetragonal symmetry allowed absorption lines for the crystal with $x=6.0$ are adequately described in terms of the available CF parameters. However, the symmetry forbidden absorption lines in our MW absorption spectra as well as the earlier magnetic data[10] can be explained only when we allow for the low-symmetry interactions, namely, the second-order terms of the monoclinic and orthorhombic CF or the Cu-Ho exchange field in the basal plane. These terms are absent for the ideal crystal and magnetic structures but might arise due to some disorder in the oxygen subsystem or a deviation of the Cu^{2+} magnetic moments from the simple collinear structure. The effect of the low-symmetry CF components is more pronounced in the absorption spectra of the crystal with $x=6.3$ revealing the increased oxygen disorder.[25]

Low-symmetry fields and inhomogeneities of one-ion and pair interaction parameters, i.e., the crystal field, exchange, and quadrupole parameters are inherent in many complex magnetic compounds. The layered perovskites $RBa_2Cu_3O_x$ may be considered as model family where the fluctuations of the crystal field are effectively controlled by the disorder in the oxygen subsystem. Our present study demonstrates that the MW absorption measurements in high magnetic fields provide a useful experimental tool to examine the low-symmetry interactions. Concluding we note the effects similar to those we studied in $HoBa_2Cu_3O_x$ are likely present in other related cuprates[26] in which the magnetic behavior is not entirely consistent with the electronic structure of the rare-earth ion in ideal crystallographic structure.

ACKNOWLEDGMENTS

This work was supported in part by the Russian Foundation for Basic Research (Project No. 10-02-00532-a), EuroMagNet II (EU under Contract No. 228043), and Project No. IAA100100803 of the Grant Agency of the AS CR.

*kazei@plms.phys.msu.ru

[1] I. K. Schuller, D. G. Hinks, M. A. Beno, D. W. Capone II, L. Soderholm, J.-P. Locquet, Y. Bruynseraede, C. U. Segre, and K. Zhang, Solid State Commun. **63**, 385 (1987).

[2] J. D. Jorgensen, M. A. Beno, D. G. Hinks, L. Soderholm, K. J. Volin, R. L. Hitterman, J. D. Grace, I. K. Schuller, C. U. Segre, K. Zhang, and M. S. Kleefisch, Phys. Rev. B **36**, 3608 (1987).

[3] P. Allenspach, A. Furrer, P. Bruesch, R. Marsolais, and P. Unternahrer, Physica C **157**, 58 (1989).

[4] A. Furrer, P. Bruesch, and P. Unternahrer, Phys. Rev. B **38**, 4616 (1988).

[5] U. Staub, J. Mesot, M. Guillaume, P. Allenspach, A. Furrer, H. Mutka, Z. Bowden, and A. Taylor, Phys. Rev. B **50**, 4068 (1994).

[6] U. Staub and L. Soderholm, in *Handbook on the Physics and Chemistry of Rare-Earths*, edited by K. A. Gschneidner, Jr., L. Eyring, and M. B. Maple (Elsevier Science B. V., Amsterdam, 2000), Vol. 30, p. 491.

[7] A. A. Martin, T. Ruf, M. Cardona, S. Jandl, D. Barba, V. Nekvasil, M. Diviš, and T. Wolf, Phys. Rev. B **59**, 6528 (1999).

[8] D. Barba, S. Jandl, V. Nekvasil, M. Maryško, M. Diviš, A. A. Martin, C. T. Lin, M. Cardona, and T. Wolf, Phys. Rev. B **63**,

054528 (2001).
[9] D. Barba, S. Jandl, V. Nekvasil, M. Maryško, K. Jurek, M. Diviš, and T. Wolf, Phys. Rev. B **69**, 024528 (2004).
[10] Z. A. Kazei, G. Fillion, A. Harat, V. V. Snegirev, and L. P. Kozeeva, J. Phys.: Condens. Matter **18**, 10445 (2006).
[11] B. Roessli, P. Fischer, U. Staub, M. Zolliker, and A. Furrer, J. Appl. Phys. **75**, 6337 (1994).
[12] E. A. Zavadskii and Yu. D. Zavorotnev, Supercond., Phys. Chem. Technol. **4**, 2113 (1991) (in Russian).
[13] Z. A. Kazei, A. A. Demidov, and N. P. Kolmakova, J. Magn. Magn. Mater. **258-259**, 590 (2003).
[14] M. Goiran, R. Klingeler, Z. A. Kazei, and V. V. Snegirev, J. Magn. Magn. Mater. **318**, 1 (2007).
[15] Ch. Krüger, K. Conder, H. Schwer, and E. Kaldis, J. Solid State Chem. **134**, 356 (1997).
[16] M. Respaud, M. Goiran, J. M. Broto, F. H. Yang, T. Ould Ely, C. Amiens, and B. Chaudret, Phys. Rev. B **59**, R3934 (1999).
[17] W. Henggeler and A. Furrer, J. Phys.: Condens. Matter **10**, 2579 (1998).
[18] J. M. Tranquada, A. H. Moudden, A. I. Goldman, P. Zolliker, D. E. Cox, G. Shirane, S. K. Sinha, D. Vaknin, D. C. Johnston, M. S. Alvarez, A. J. Jacobson, J. T. Lewandowski, and J. M. Newsam, Phys. Rev. B **38**, 2477 (1988).
[19] J. M. Tranquada, D. E. Cox, W. Kunnmann, H. Moudden, G. Shirane, M. Suenaga, P. Zolliker, D. Vaknin, S. K. Sinha, M. S. Alvarez, A. J. Jacobson, and D. C. Johnston, Phys. Rev. Lett. **60**, 156 (1988).
[20] H. Kadowaki, M. Nishi, Y. Yamada, H. Takeya, H. Takei, S. M. Shapiro, and G. Shirane, Phys. Rev. B **37**, 7932 (1988).
[21] V. Nekvasil, Solid State Commun. **65**, 1103 (1988).
[22] P. Allenspach, A. Furrer, and F. Hulliger, Phys. Rev. B **39**, 2226 (1989).
[23] P. Morin, J. Rouchy, and Z. Kazei, Phys. Rev. B **51**, 15103 (1995).
[24] S. Skanthakumar, H. Zhang, T. W. Clinton, W.-H. Li, J. W. Lynn, Z. Fisk, and S.-W. Cheong, Physica C **160**, 124 (1989).
[25] W. Pickett, Rev. Mod. Phys. **61**, 433 (1989).
[26] L. Soderholm, C.-K. Loong, U. Staub, S. Skanthakumar, J. Simon Xue, J. P. Hammonds, J. E. Greedan, and M. Maric, Physica C **246**, 11 (1995).